

On the Performance Limits of Agrivoltaics—From Thermodynamic to Geo-Meteorological Considerations

Austin M. Kay,* Drew B. Riley, Oskar J. Sandberg, Gregory Burwell, Paul Meredith,* and Ardalan Armin*


As the world strives toward its net-zero targets, innovative solutions are required to reduce carbon emissions across all industrial sectors. One approach that can reduce emissions from food production is agrivoltaics—photovoltaic devices that enable the dual-use of land for both agricultural and electrical power-generating purposes. Optimizing agrivoltaics presents a complex systems-level challenge requiring a balance between maximizing crop yields and on-site power generation. This balance necessitates careful consideration of optics (light absorption, reflection, and transmission), thermodynamics, and the efficiency at which light is converted into electricity. Herein, real-world solar insolation and temperature data are used in combination with a comprehensive device-level model to determine the annual power generation of agrivoltaics based on different photovoltaic material choices. It is found that organic semiconductor-based photovoltaics integrated as semitransparent elements of protected cropping environments (advanced greenhouses) have comparable performance to state-of-the-art, inorganic semiconductor-based photovoltaics like silicon. The results provide a solid technical basis for building full, systems-level, technoeconomic models that account for crop and location requirements, starting from the undeniable standpoint of thermodynamics and electro-optical physics.

1. Introduction

Throughout the last decade, rapid progress has been made with next-generation photovoltaics (PVs) based on organic

A. M. Kay, D. B. Riley, G. Burwell, P. Meredith, A. Armin
Sustainable Advanced Materials Group (Sêr-SAM)
Centre for Integrative Semiconductor Materials (CISM)
Department of Physics
Swansea University Bay Campus
Swansea SA1 8EN, UK
E-mail: a.m.kay.954708@swansea.ac.uk; paul.meredith@swansea.ac.uk;
ardalan.armin@swansea.ac.uk

O. J. Sandberg
Department of Physics
Faculty of Science and Engineering
Åbo Akademi University
20500 Turku, Finland

 The ORCID identification number(s) for the author(s) of this article can be found under <https://doi.org/10.1002/solr.202400456>.

© 2024 The Author(s). Solar RRL published by Wiley-VCH GmbH. This is an open access article under the terms of the Creative Commons Attribution License, which permits use, distribution and reproduction in any medium, provided the original work is properly cited.

DOI: 10.1002/solr.202400456

semiconductors and perovskites, including single-junction power conversion efficiencies (PCEs) nearing and surpassing 20% for these materials, respectively.^[1–3] In addition, the unique attributes these lightweight materials possess, including solution-processibility, mechanical flexibility, and tunable optical properties, enable new “application-targeted” opportunities. Such applications include indoor PVs for powering Internet-of-Things devices,^[4–6] building-integrated photovoltaics (such as PV window panes),^[7] and space-based solar cells.^[8,9]

One application that could play a pivotal role in the global decarbonization effort is “agrivoltaics,” through which valuable real-estate is shared between agriculture and power-generation.^[10–12] By integrating PVs into agricultural infrastructure—with light-weight organic semiconductor-based and perovskite-based PVs being particularly suitable for retrofitting weaker/older structures—agrivoltaics could alleviate the

pressing challenge of sustainably feeding the world’s growing population in the face of extreme weather events, land scarcity, and dwindling resources, all while simultaneously increasing energy production.^[13] Indeed, it is expected that by covering just 1% of its current agricultural area with agrivoltaics, the European Union could meet its PV capacity targets for the year 2030 with these devices alone.^[14] To meet the demand for PV fabrication on such a large-scale, high-throughput, low-embodied energy fabrication techniques such as roll-to-roll printing and slot-die coating are ideal. These techniques make use of the solution-processibility and flexibility of organic semiconductors and perovskites, allowing for the fabrication of large-area, ultra-thin devices using less energy than what is required to fabricate their inorganic PV counterparts.^[15–17] These factors play a vital role in the decarbonization of the energy sector, and the circular economy of PVs as a whole.^[18,19]

A notable innovation in the field of agrivoltaics is the use of lightweight, semitransparent PVs, with three exemplary applications illustrated in **Figure 1**.^[20–23] Figure 1a shows how semitransparent PVs can be integrated into the roofs and walls of protected cropping environments, such as advanced greenhouses, to provide electrical energy for the climate control systems within, thereby reducing carbon emissions.^[24] Compared with traditional field farming methods, protected cropping

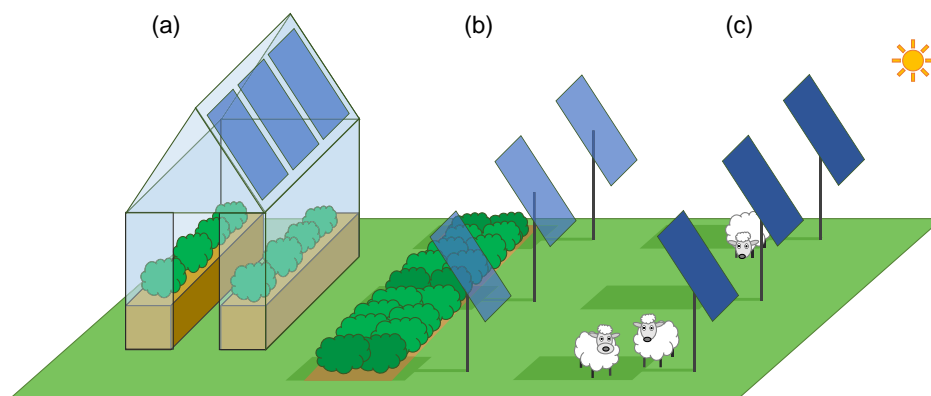


Figure 1. Three exemplary applications of agrivoltaics. a) A protected cropping environment, such as an advanced greenhouse, in which lightweight, semitransparent PV cells integrated into the roof and/or walls may be used to, e.g., offset the carbon footprint of sensors and climate control systems within. Semitransparent PVs and opaque PVs can also be combined with open cropping environments and livestock, providing shade while also generating power, as illustrated in (b) and (c), respectively.

environments offer better control over environmental conditions, enable year-round cultivation, minimize water consumption, reduce transmission of disease and pests, and ultimately improve crop yield.^[25,26] Figure 1b, meanwhile, illustrates how arrays of semitransparent PVs may be used to shelter crops in open cropping environments. Additionally, these arrays can be used to shelter livestock, as illustrated in Figure 1c, though this approach could be (and is) implemented with opaque PVs such as silicon and cadmium telluride (CdTe) at commercial/industrial scales, particularly in high solar insolation geographies.^[26] In either case, a symbiosis between the PV arrays and the crops or livestock is ideal; indeed, the introduction of flocks of sheep to ground-mounted PV arrays has been found to reduce maintenance costs.^[12,27]

One key question that frontier research currently seeks to answer is how integrating agrivoltaics into industrial cropping environments will affect crop yields. This is an important consideration as vital processes, such as photosynthesis and photomorphogenesis, can be sensitive not only to temperature, partial pressure of carbon dioxide, humidity, nutrient levels, and soil pH, but also variations in the wavelength, intensity, and photoperiod of the photosynthetically-active radiation, be it natural or artificial in origin.^[28–32] The illumination conditions in protected or closed environments must also be considered from the perspective of any insect pollinators (an example being the dependence of bee vision on ultraviolet light^[33,34]). Hence, the spectral properties and intensity of light transmitted by semitransparent agrivoltaics (not just the light absorbed to create electricity) are central design considerations. This is illustrated by way of example in **Figure 2**, wherein the irradiance (I_{source}) of sunlight is plotted in **Figure 2a**, while the absorbances of plant chlorophylls (the primary absorbers and photochemical energy providers in photosynthesis) and bee photoreceptors are plotted in **Figure 2b,c**, respectively.^[20–22,28,33,34]

To collect as much light for power generation as possible, while avoiding the wavelengths that chlorophylls depend on, the absorbance of an agrivoltaic device (Abs) must be minimal for photons of energy $E > 1.77$ eV, while the corresponding spectral transmission function (T) must simultaneously be maximized. Due to this interplay between $T(E)$ and $\text{Abs}(E)$, there is

an undoubted trade-off between crop yield and power generation. While this trade-off has been empirically explored for limited crop types,^[35] to our knowledge, there is not yet a comprehensive and accurate device-level model to predict the thermodynamic performance limits of various semiconductors for semitransparent agrivoltaics. This would be particularly valuable for molecular semiconductors such as organics and perovskites, wherein tunable bandgaps and electro-optics can be manipulated and engineered.^[36,37]

In this work, the thermodynamic limits of organic semiconductor-based photovoltaics (OPVs) are explored, and their performance as agrivoltaics devices is predicted from first principles. These lightweight devices consist of submicron photoactive layers with blends of at least two molecular components, which are typically an electron-donating polymer (the donor) and an electron-accepting small molecule (the acceptor). As the primary photoexcitations in OPVs are electron–hole pairs, or excitons, which remain coulombically-bound due to the inherently low dielectric constants,^[38,39] two or more molecular components are needed to separate and collect the free charges via the formation of interfacial charge-transfer states.^[40] Improvements in morphological, energetic, and kinetic properties of OPV materials, including reduced energetic disorder and nonradiative recombination, continue to pave the way toward higher performance, with PCEs of single-junction OPVs reaching up to 20% in recent years.^[41–47] These high PCEs can also be attributed to the advent of small-molecule, nonfullerene acceptors (NFAs).^[48,49] We focus our investigation on OPVs as their optical properties can be tuned by altering their molecular structure—an extremely desirable attribute that could allow specific OPV materials to be coupled with certain crops. We note that perovskite semiconductor-based PVs, to an extent, have similar properties that also make them promising candidates for agrivoltaic applications, and thus this current work has wider relevance.^[17,21,50–53]

To begin, we first establish realistic performance limits expected for OPVs under AM1.5G illumination, which is the global test standard by which PV technologies are compared. We achieve this by accounting for the various loss mechanisms associated with OPVs, including radiative open-circuit voltage losses induced by subgap absorption, and nonradiative

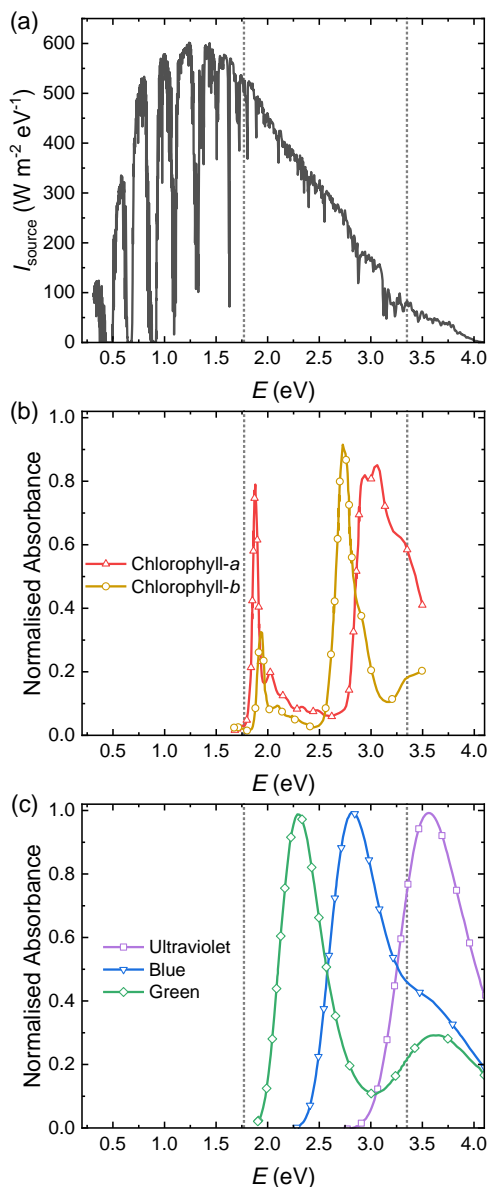


Figure 2. Optical considerations for semitransparent agrivoltaics in open and protected cropping environments. a) The standard AM1.5 G spectrum for sunlight (with integrated spectral irradiance $P_{\text{source}} = \int_0^\infty I_{\text{source}}(E) dE = 1000 \text{ W m}^{-2}$) plotted as a function of the photon energy (E). b) The normalized absorbance spectra of chlorophyll-*a* and chlorophyll-*b*—the primary energy sources for photosynthesis—plotted against the photon energy.^[20,21,28] c) The normalized absorbance spectra of bees' ultraviolet, blue, and green photoreceptors.^[33,34] In all panels, the vertical dashed lines approximately indicate the lower (1.77 eV) and upper (3.35 eV) bounds of the visible region of the electromagnetic spectrum.

open-circuit voltage losses. Following this, we systematically add complexity to probe factors limiting the performance of semitransparent systems. This includes a study on the trade-off between light transmission and the performance of semitransparent PVs in the thermodynamic limit. While the former is determined using optical transfer matrix modeling,^[54–58] the latter is evaluated using our open-source “Photovoltaic

Performance Simulator” (PV-Sim) tool, which is available online.^[59,60] By defining a coverage factor (CF) with which PV cells occupy the area of a protected cropping structure, we then find that the light-utilization efficiency (LUE), quantifying the amount of incident light converted to electrical power by PVs or made available to crops, of semitransparent agrivoltaics based on OPVs is comparable with that of opaque solar cells based on inorganic semiconductors like crystalline silicon or gallium arsenide.^[44] Finally, we incorporate geographical and meteorological considerations by evaluating the annual output of agrivoltaics based on different semiconductor materials using real-world solar irradiance and temperature data. To empower other researchers with the ability to carry out similar investigations, we have upgraded our PV-Sim tool to include a user interface for simulating PV performance using real-world irradiance and temperature data, as well as device-level parameters (such as nonradiative open-circuit voltage losses, series resistances, shunt resistances, and more).

Our research primarily aims to determine the thermodynamic limit of LUE achievable with molecular semiconductors, while intentionally omitting cost considerations and specific crop constraints—but we note that a fundamental device-level model must be the starting point for full techno-economic and systems-level optimization.

2. Results and Discussion

2.1. The Thermodynamic Limit

To provide a baseline for our investigation, we start by establishing the thermodynamic limit of OPV performance under AM1.5 G illumination. To this end, a methodology detailed in our prior work is used to determine the PCE.^[60] For a brief summary of this methodology, including the incorporation of intrinsic features such as band-filling and nonradiative open-circuit voltage losses, as well as device-level parameters such as the series and shunt resistances, see Section S1 of the Supporting Information.

In the most ideal case, the PCE may be determined by assuming the semiconductor has abrupt, well-defined band edges. In this case, the PV external quantum efficiency (EQE_{PV}), which is defined as the product of the absorbance, $\text{Abs}(E)$, and the internal quantum efficiency of photoexcitation-to-collected charge conversion, $\text{IQE}(E)$, can be modeled as a step function around some threshold optical gap (E_{opt}):

$$\text{EQE}_{\text{PV}}(E) = \begin{cases} \text{EQE}_{\text{max}}, & \text{if } E \geq E_{\text{opt}} \\ 0, & \text{otherwise} \end{cases} \quad (1)$$

Here, EQE_{max} is the above-gap PV quantum efficiency. Equation (1) reduces to the Shockley–Queisser (SQ) model of a single-junction solar cell in the ideal case that 1) each photon generates exactly one collected electron–hole pair that is perfectly extracted, giving $\text{EQE}_{\text{max}} = \text{IQE} = 1$, and 2) recombination is purely radiative.^[61]

A step-function EQE_{PV} spectrum is exemplified for $E_{\text{opt}} = 1.50 \text{ eV}$ by the black curve in **Figure 3a**. The corresponding PCE under AM1.5 G illumination is plotted against the

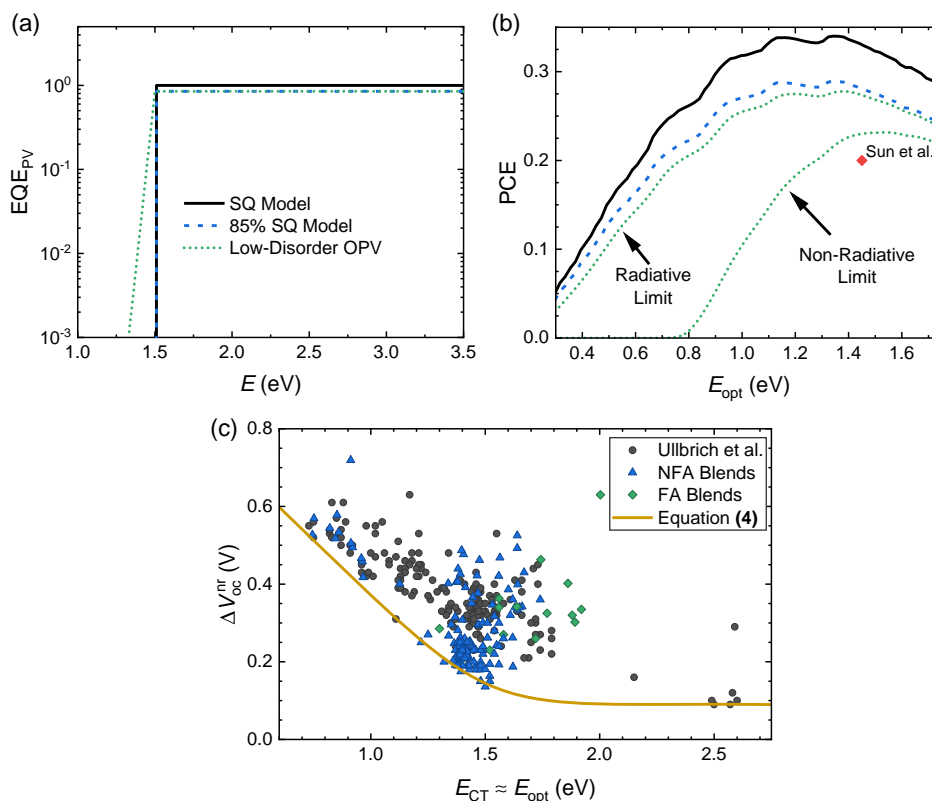


Figure 3. The thermodynamic limit of the PCE in three models: the SQ model (solid black lines), a step function EQE_{PV} with $\text{EQE}_{\text{max}} = 85\%$ (dashed blue lines), and a realistic low-disorder OPV model (dotted green lines). a) The EQE_{PV} spectra for these three models plotted as a function of the photon energy E using an optical gap $E_{\text{opt}} = 1.5$ eV. b) The corresponding PCEs plotted as a function of the optical gap. Note that both the radiative and nonradiative limits of the PCE are plotted for the low-disorder OPV model, where the nonradiative open-circuit voltage losses were determined in the latter case using Equation (4). The red diamond indicates one of the highest PCEs achieved using a single junction OPV, which was recently published by Sun et al.^[47] c) Nonradiative open-circuit voltage losses ($\Delta V_{\text{oc}}^{\text{nr}}$) in OPVs, plotted as a function of the energy of the charge-transfer state, which can be approximated with the optical gap in low-offset, NFA blends. Here, the black circles illustrate data compiled by Ullbrich et al.^[70] while the blue triangles and green diamonds indicate $\Delta V_{\text{oc}}^{\text{nr}}$ in NFA and fullerene acceptor (FA) systems, respectively (tabulated data provided in Section S4 of the Supporting Information).^[60,72–81]

optical gap in Figure 3b. In both panels, additional curves are shown which were simulated using $\text{EQE}_{\text{max}} = 0.85$; a more realistic value seen for many state-of-the-art OPVs due to the various loss mechanisms associated with these materials, including transport losses. Based on this reduction in EQE_{max} , an optimal solar cell with minimal voltage losses and an ideal optical gap (between around 1 eV and 1.5 eV) could generate power at a maximum efficiency of around 28%. However, the prevalence of intrinsic loss mechanisms in PV materials, such as radiative open-circuit voltage losses and nonradiative recombination, will further lower this limit.^[42,62,63] To predict the maximum efficiency of an OPV device more realistically, we, therefore, include radiative open-circuit voltage losses ($\Delta V_{\text{oc}}^{\text{rad}}$) by accounting for subgap absorption. To this end, we describe a low-static energetic disorder OPV material by replacing the abrupt edge of the step function EQE_{PV} with a subgap tail (known as an Urbach tail) of the form:^[64–66]

$$\text{EQE}_{\text{PV}}(E) \approx \text{EQE}_{\text{max}} \begin{cases} \exp\left(\frac{E - E_{\text{opt}}}{k_{\text{B}} T_{\text{PV}}}\right), & \text{if } E \leq E_{\text{opt}} \\ 1, & \text{otherwise} \end{cases} \quad (2)$$

A discussion on the quantification and effect of static energetic disorder in OPVs is presented in Section S2 of the Supporting Information. In Equation (2), k_{B} denotes the Boltzmann constant and T_{PV} is the PV cell's temperature, which we assume is $20^\circ\text{C} = 293.15$ K for now. The operational temperature of an agrivoltaic device can, in practice, be higher than this. However, as we show in Section S3 of the Supporting Information, even at $T_{\text{PV}} = 50^\circ\text{C} = 323.15$ K only a small loss in PCE is obtained in the thermodynamic limit. Note that, in Equation (2), the subgap tail has a characteristic Urbach energy (E_{U}) equal to the thermal energy, $k_{\text{B}} T_{\text{PV}}$.^[66] We emphasize that Equation (2) applies to low-offset OPV systems with low static energetic disorder, providing a good approximation for state-of-the-art NFA-based OPVs.^[65,66] As illustrated in Figure 3, accounting for subgap absorption using Equation (2) leads to a further loss in device performance due to the increased dark saturation current, leading to a reduction in the radiative open-circuit voltage ($V_{\text{oc}}^{\text{rad}}$) of the device, as $V_{\text{oc}}^{\text{rad}} = V_{\text{oc}}^{\text{SQ}} - \Delta V_{\text{oc}}^{\text{rad}}$.^[60] Here, $V_{\text{oc}}^{\text{SQ}}$ is the open-circuit voltage in the SQ model, while the $\Delta V_{\text{oc}}^{\text{rad}}$ induced by a subgap EQE_{PV} tail with $E_{\text{U}} = k_{\text{B}} T_{\text{PV}}$ can be estimated through^[60]

$$q\Delta V_{oc}^{rad} = k_B T_{PV} \ln\left(\frac{E_{opt}}{3k_B T_{PV}} + 1\right) + k_B T_{PV} \ln\left(1 - \left[\frac{qV_{oc}}{E_{opt}}\right]^3\right) \quad (3)$$

where the right-hand term arises when accounting for band-filling effects and the chemical potential of light.^[60,67–69]

To make a more realistic prediction for the PCE of OPVs, one might account for their intrinsic nonradiative open-circuit voltage losses (ΔV_{oc}^{nr}) that generally decrease with increasing E_{opt} .^[62,70,71] This so-called energy-gap law is made apparent by the ΔV_{oc}^{nr} data of OPV systems from the literature (including state-of-the-art devices), which are plotted against E_{opt} in Figure 3c (see Section S4 of the Supporting Information).^[60,70,72–81] A real OPV device's open-circuit voltage relates to ΔV_{oc}^{nr} through $V_{oc} = V_{oc}^{rad} - \Delta V_{oc}^{nr}$, where ΔV_{oc}^{nr} may be determined either through electroluminescent EQE measurements,^[82] or through EQE_{PV} measurements.^[60,83] To empirically estimate the expected ΔV_{oc}^{nr} for a given E_{opt} , ΔV_{oc}^{nr} can be approximated as

$$\Delta V_{oc}^{nr}(E_{opt}) = \Delta V_0 \left[\frac{\varepsilon - E_{opt}}{1 - \exp(-r[\varepsilon - E_{opt}])} + \delta \right] \quad (4)$$

where E_{opt} has units of eV, $\Delta V_0 = 0.57 \text{ V eV}^{-1}$, $\varepsilon = 1.49 \text{ eV}$, $r = 10 \text{ eV}^{-1}$, and $\delta = 0.16 \text{ eV}$. We stress that Equation (4) has no theoretical origin but is just a means of capturing trends observed in current state-of-the-art ΔV_{oc}^{nr} data. Expressions for $\Delta V_{oc}^{nr}(E_{opt})$ in OPVs that have been determined using more robust theoretical frameworks can be found in works by Azzouzi et al. and Chen et al.^[62,71] After including both radiative open-circuit voltage losses (through sub-gap absorption) and nonradiative open-circuit voltage losses using Equation (4), the maximum PCE for a low-disorder OPV device in the nonradiative limit is reduced to around 23% under AM1.5 G illumination, with the best-performing optical gap at 1.54 eV. For reference, the high PCE recently obtained for a single-junction OPV device by Sun et al. is compared with this nonradiative limit in Figure 3b.^[47]

2.2. Trade-Off between Light Transmission and PV Performance

With the baseline established, we next investigated the trade-off between absorption and transmission of light by first defining the LUE of a semitransparent agrivoltaic device as $LUE = PCE \times AVT$.^[84] This metric quantifies how much of the incident light is converted to electrical power by the semitransparent PVs, or transmitted through them and made available to the crops on the other side. To calculate it, the average visible transmission (AVT) must first be calculated using:

$$AVT \approx \frac{1}{1.58 \text{ eV}} \int_{1.77 \text{ eV}}^{3.35 \text{ eV}} [1 - \text{Abs}(E) - R(E)] dE \quad (5)$$

Here $R(E)$ is the OPV device's reflectance, which we assume, for now, to be zero at all photon energies, corresponding to a PV device with a good antireflection (AR) coating. Retaining the assumption of a spectrally flat, near-unity IQE, then $\text{Abs}(E) = EQE_{PV}(E)$ holds true. To define the AVT using Equation (5), we purposefully used a step function across the visible region of the electromagnetic spectrum, thereby treating all

photon energies as equally important. In the past, the spectral response of the human eye has been used to weight the AVT, similar to how it is used to inform building-integrated PVs.^[85–88] For agrivoltaic applications, however, the needs of the crops and any insect pollinators are different; thus, by treating all visible wavelengths equally, we remain agnostic to any particular crop type. As we explore in Section S5 of the Supporting Information, more complex weightings could, in principle, be used to account for the wavelength-selectivity of a particular crop type and the spectral properties of different OPV materials, as previously highlighted by Zhao et al.^[22,89]

With the definition of the LUE in hand, we investigated the trade-off between absorption and transmission by reducing the low-disorder OPV device's EQE_{PV} (dotted, green curves in Figure 3) in the visible region of the electromagnetic spectrum (around 370–700 nm, or 1.77–3.35 eV). The result of this analysis is illustrated in Figure 4. Therein, the effect of reducing the visible region EQE_{PV} from 85% to 0% is illustrated (for $E_{opt} = 1.50 \text{ eV}$) in Figure 4a, with the resulting transmission spectra plotted in Figure 4b. As expected, reducing the absorption in the visible region leads to increased transmission.

Using visible region-reduced EQE_{PV} spectra, the PCE was determined as a function of E_{opt} in the radiative and nonradiative limits, with the results plotted in Figure 4c,d, respectively. Note that, in the latter case, nonradiative open-circuit voltage losses were accounted for using Equation (4). These PCE curves were used to plot the LUE as a function of E_{opt} in the radiative and nonradiative limits, with the resultant curves shown in Figure 4e,f, respectively. Based on these curves, it is evident that increasing the AVT from 15% to 100% (or, equivalently, reducing EQE_{max} from 85% to 0%) causes the maximum radiative-limit PCE to reduce from 28% to 15%. Similarly, in the nonradiative limit, the maximum PCE is reduced from roughly 23% to 9%. Despite this, the trade-off between light transmission and power generation requires that the visible region EQE_{PV} be as minimal as possible for optimal agrivoltaic performance, as shown by the LUE curves in Figure 4e. In the realistic case that includes nonradiative losses (Figure 4f), the maximum LUE is 9.8%, assuming $AVT = 0.75$ and $1.2 \leq E_{opt} \leq 1.5 \text{ eV}$. This, however, is only a first approximation. To estimate the LUEs of typical agrivoltaic devices with higher accuracy, a more thorough description of the spectral behavior of their transmission, reflection, and absorption is needed.

2.3. Realistic Absorption without Cavity Effects or Reflectance

To predict the LUEs of semitransparent OPVs more accurately, the optical constants of the constituent layers can be used to simulate their absorbance spectra. Neglecting, for now, the cavity effects that arise from back-reflection and optical interference in thin-film PVs, then to a first-order approximation the device's EQE_{PV} spectrum can be related to the absorption coefficient, $\alpha(E)$, of the photo-active layer of thickness d via a Beer-Lambert-like expression of the form:^[65]

$$EQE_{PV}(E) = EQE_{max}[1 - e^{-\alpha(E)d}] \quad (6)$$

The prefactor EQE_{max} generally relates to the IQE and the intensity transmission into the OPV active layer.^[54] A full,

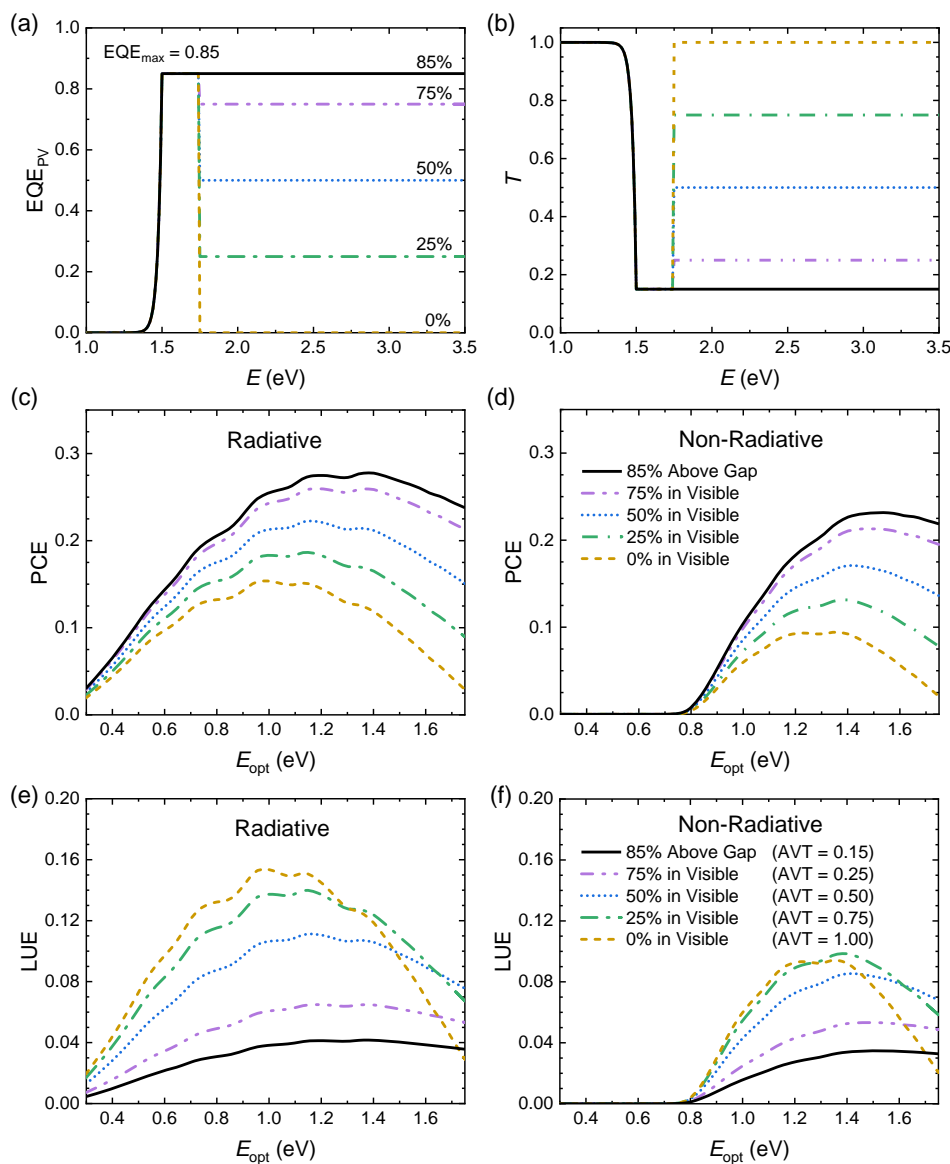


Figure 4. Comparing the effect of reducing the EQE_{PV} in the visible region on the LUEs of idealized, low-disorder OPVs. a) EQE_{PV} spectra modeled using Equation (2) with $E_{opt} = 1.5$ eV and (black line) $EQE_{max} = 0.85$, and (colored dashed-lines) reduced EQE_{max} in the visible region, note that all curves have exponentially-decaying subgap EQE_{PV} tails with Urbach energy $E_U = k_B T_{PV} \approx 25.3$ meV. b) The corresponding spectral intensity transmission $T(E)$, assuming that the reflectance $R(E)$ is negligible. c) The thermodynamic limit PCEs as a function of optical gap in the radiative and d) nonradiative limits. e) The corresponding radiative and f) nonradiative LUEs as a function of optical gap.

optically modeled treatment, including back-reflection and optical cavity effects, is presented in the next section. To model the absorption of the photoactive layer of an example OPV device, we use $\alpha(E)$ of ‘Y6’,^[90] a state-of-the-art, small-molecule, NFA. We consider this absorption coefficient in particular as its spectral line shape—including a peak and a trough in the near-infrared and visible regions, respectively—closely resembles the idealized EQE_{PV} spectra in Figure 4a. We emphasize that we are not considering the performance of a Y6-only OPV device, which would be poor (as it lacks a donor component), but are instead considering the thermodynamic limits of an OPV device with an absorption coefficient resembling that of Y6, which is

shown in Figure 5a. The EQE_{PV} spectra simulated using Equation (6) are illustrated in Figure 5b, with the corresponding intensity transmission spectra determined using $T(E) \approx 1 - EQE_{PV}(E)$ plotted in Figure 5c. From Figure 5b,c, it can be seen that as d is increased, EQE_{PV} approaches its above-gap saturation value ($EQE_{max} = 0.85$, in this case) while the AVT concurrently decreases. Figure 5d shows the resultant PCE, AVT, and LUE as a function of d . Due to increased absorption, the PCE gradually increases with d while the AVT decreases. This trade-off between power generation and light transmission leads to a maximum LUE of 7.8% at $d \approx 100$ nm. Note that, in these calculations, a nonradiative open-circuit voltage loss

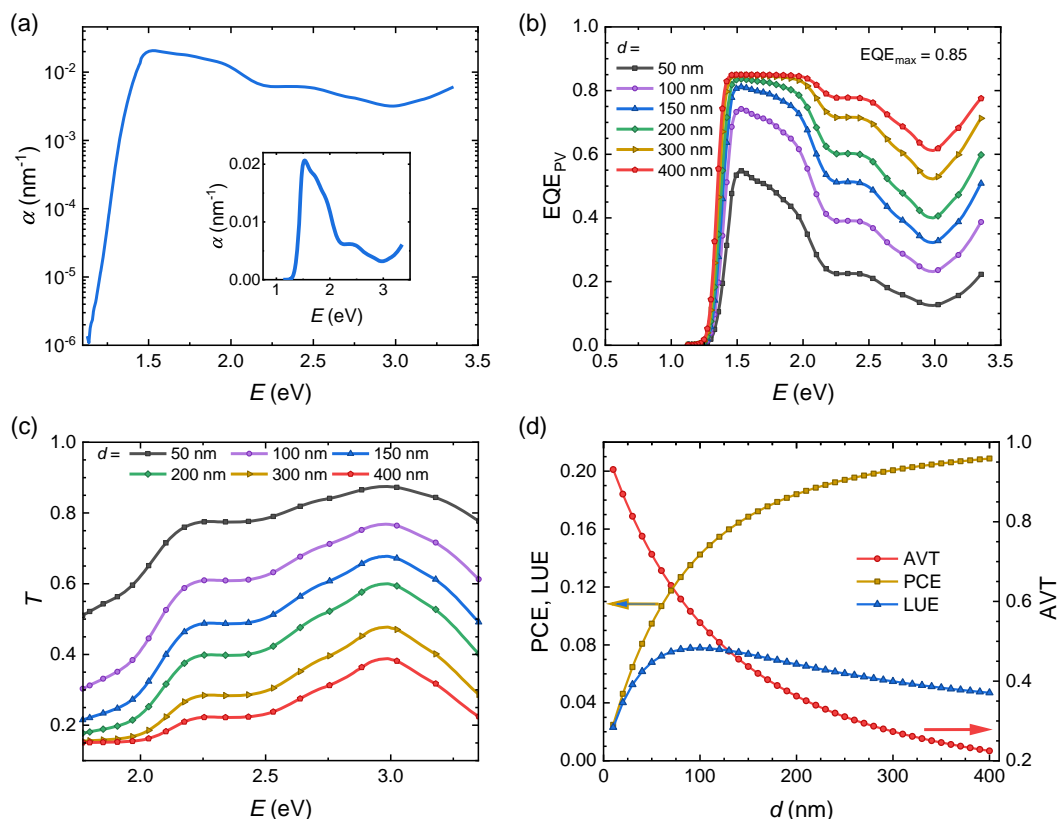


Figure 5. Thickness-dependent agrivoltaic performance of an OPV system modeled on a) the absorption coefficient (α) of Y6 with $E_{\text{opt}} \approx 1.4$ eV.^[90] b) EQE_{PV} spectra simulated for a variety of active layer thicknesses (d) using the absorption coefficient from (a) and a realistic above-gap quantum efficiency $\text{EQE}_{\text{max}} = 0.85$. c) The corresponding transmission spectra in the visible region, determined in the case of negligible reflectance using $T(E) \approx 1 - \text{EQE}_{\text{PV}}(E)$. d) The obtained PCE, AVT, and $\text{LUE} = \text{PCE} \times \text{AVT}$, plotted as a function of d .

$\Delta V_{\text{oc}}^{\text{nr}} \approx 0.177$ V was assigned using Equation (4), as $\frac{\partial \alpha(E)}{\partial E} = 0$ leads to $E_{\text{opt}} \approx 1.4$ eV for the Y6 active layer.

2.4. Optically Modeled Absorption with Cavity Effects and Reflectance

The assumption of minimal back-reflection in semitransparent OPV devices, which underpins Equation (6), does not account for changes in the line shape of the EQE_{PV} due to the optical interference effects that arise inside thin-film PVs and other related electro-optical device structures.^[54–58] To determine the LUEs of agrivoltaic devices more accurately, their EQE_{PV} spectra were simulated by adapting an optical transfer matrix model that has been applied extensively in the past (see Section S6 of the Supporting Information).^[54–58] Note that two key assumptions are made in this model: first, the albedo effect of the environment's content is assumed to be minimal, such that most of the light is either scattered or absorbed after passing through the semitransparent PV device (and minimally reflected back into the reverse side of the device); accounting for reflected direct and diffuse light using bifacial PV devices could increase energy generation by up to 20–25%.^[91–94] The second assumption made here is that sunlight impinges the device at normal incidence; if

this were not the case, the reflectance of the device would likely be greater due to the Fresnel angular dependencies.^[95]

Figure 6a shows a typical device structure for a semitransparent OPV device. Therein, indium tin oxide (ITO) acts as a semi-transparent contact on a 1 mm thick glass substrate, while zinc oxide (ZnO) and molybdenum oxide (MoO_3) form electron and hole transport layers, respectively, either side of the photo-active junction. We used the optical constants of Y6 to describe the active layer of this model structure and emphasize, once again, that this is because the spectral line shape of its absorption coefficient is close to the optimal EQE_{PV} shown in Figure 4a. The device is complete with a second semitransparent ITO layer as the bottom contact. Using this device architecture, the EQE_{PV} spectra shown in Figure 6b were simulated for varied d using the optical transfer matrix model; as the active layer thickness increases, the above-gap quantum efficiency saturates to $\text{EQE}_{\text{max}} \approx 0.80$. The corresponding reflectance R and transmission T are plotted in Figure 6c, with the resultant AVT, PCE, and LUE plotted versus d in Figure 6d. Note that the PCE was evaluated in the nonradiative limit by assigning $\Delta V_{\text{oc}}^{\text{nr}} \approx 0.177$ V to the active layer (modeled on Y6's optical constants) with $E_{\text{opt}} \approx 1.4$ eV using Equation (4). From Figure 6, the trade-off between increasing PCE and decreasing AVT with d results in an optimal $\text{LUE} \approx 4.9\%$ for $d = 100$ nm. In addition, the effects

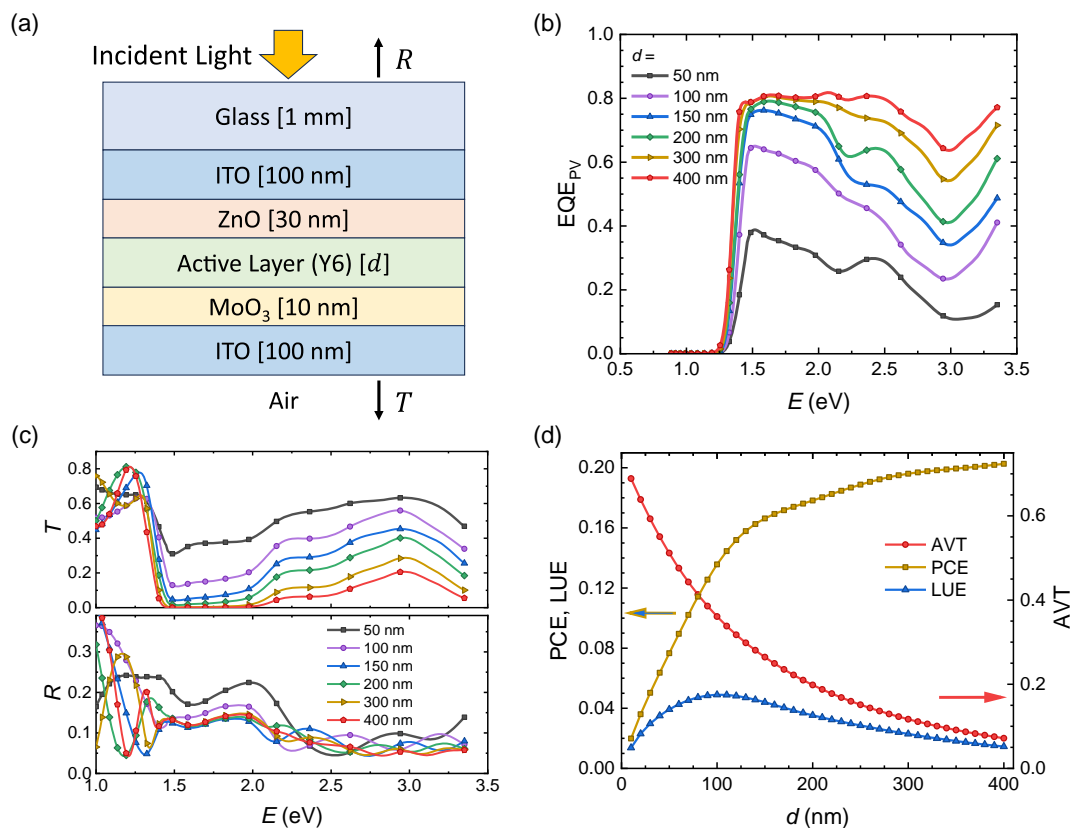


Figure 6. Simulating the LUE of a semitransparent OPV device using an optical transfer matrix model.^[57,58] a) The architecture used to model a semitransparent OPV, where the thicknesses of each of the layers are inset. The active layer's optical constants are modeled on Y6. b) The EQE_{PV} spectra determined using the optical model, plotted as a function of the incident photon energy E . Note that a unity IQE has been assumed. c) The corresponding transmittance $T(E)$ and reflectance $R(E)$ of the device. d) The PCE, AVT, and LUE, plotted as a function of the active layer thickness d .

of optical interference in the thin-film cavity are apparent, with the obtained PCE fluctuating with increasing d when compared with Figure 5d.

2.5. Comparison with Opaque, Inorganic Solar Cells

To evaluate the real-world applicability of semitransparent OPVs, their calculated LUEs were compared with the LUEs of opaque solar cells based on inorganic semiconductors (notably silicon, III–V, and chalcogenides) that are spaced apart (allowing light into the protected cropping environment between panels). This approach to integrating PV into a building's structural fabric (including agricultural environments) could be viewed as the standard analogous comparator to the more “engineered” solution of semitransparent bandgap-tuned approach afforded by molecular semiconductors. We limit this comparator investigation to monofacial PV cells (i.e., solar cells harvesting light on one side only) as the albedo effect of the contents of the cropping environment, including crops and soil, is a complex and site-specific problem to be modeled at the systems-level. For example, parameters like humidity, temperature, and even surface roughness and moisture content of the soil can affect the amount of light reflected back toward a bifacial PV cell, as well as the absorbance of the cell itself.^[96–98] We would therefore acknowledge

that bifacial cells could be more ideal for agrivoltaic applications.^[93,94,99] Though an accurate investigation into the performance of bifacial cells is somewhat out of the scope of this investigation, albedo effects will slightly increase the absorbance and PCE of semitransparent PVs (which, by nature, allow light to enter from *both* sides of the device), as we explore in Section S7 of the Supporting Information.

To compare the performance of monofacial, semitransparent OPVs with opaque, inorganic PV cells, we define a PV CF as the ratio of the area covered by PVs (A_{PV}) to the full area of the agrivoltaic roof/panel (A_{roof}):

$$CF = \frac{A_{PV}}{A_{roof}} \quad (7)$$

The calculation of the CF is schematically illustrated for vertically arranged strips of cells in Figure 7a, though, in principle, any geometric combination of cells could be used. Using the CF, a weighted LUE that accounts for the photoactive area of an agrivoltaic roof can be defined as:

$$LUE_{CF} = CF \times AVT \times PCE \quad (8)$$

Using this equation, in Figure 7b the CF-weighted LUEs have been determined and plotted for a variety of state-of-the-art,

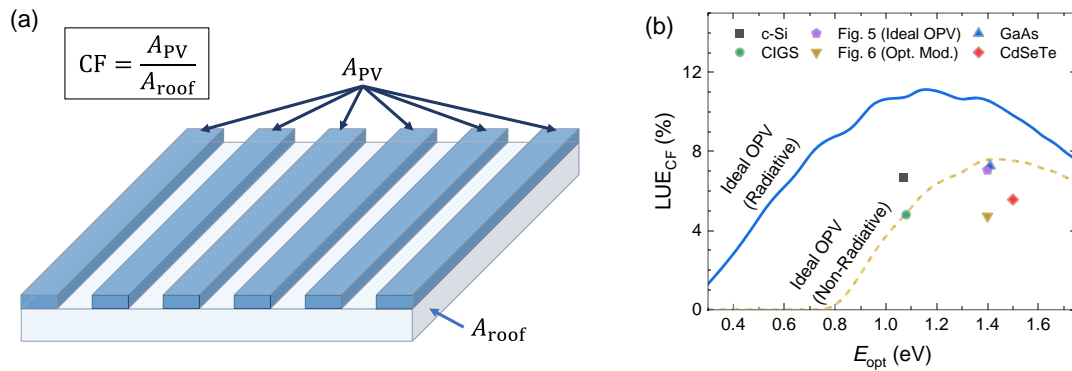


Figure 7. a) Calculation of the coverage factor (CF) and b) the CF-weighted LUE (LUE_{CF}) for a handful of state-of-the-art, single-junction PV cells based on inorganic semiconductors,^[44] which are plotted alongside the LUEs for the idealized, low-disorder OPV system from Figure 5 and the corresponding optically modeled (opt. mod.) device from Figure 6. For reference, the CF-weighted LUE in the radiative and nonradiative limits of the ideal, low-disorder OPV model are plotted as a function of the optical gap (with $EQE_{max} = 0.85$) as a blue curve and a dashed gold curve, respectively.

inorganic solar cells, assuming 50% CFs. These materials included crystalline silicon (c-Si), gallium arsenide (GaAs), selenium-doped cadmium telluride (CdSeTe),^[100] and copper indium gallium selenide (CIGS).^[44] The 50% CF assigned to these materials gives a 50% AVT across the full area of the roof, provided that 100% of the light is transmitted in the uncovered areas and 0% is transmitted in the covered areas (i.e., assuming the cells are opaque). A 50% CF was selected as it maximizes the CF-weighted LUE in the case that reflectance is negligible (from substituting $AVT \approx 1 - CF$ into Equation (8) and finding the stationary point with respect to CF).

Also plotted in Figure 7b are the highest CF-weighted LUEs obtained for the idealized, low-disorder OPV device considered in Figure 5, and the optically modeled device considered in Figure 6. In both cases, the semitransparent OPV cells are assumed to cover 100% of the roof ($CF = 1$). Based on this figure, one can see that LUE_{CF} for the optimal-thickness, low-disorder OPV device from Figure 5 ($LUE_{CF} \approx 7.8\%$; $AVT = 0.55$) surpasses LUE_{CF} for most state-of-the-art inorganic solar cells, though it is assumed to have negligible reflectance. In contrast, the optimal thickness, optically modeled device from Figure 6 ($LUE_{CF} \approx 4.9\%$; $AVT = 0.36$) is on par with state-of-the-art CIGS and CdTe cells. We note again that the ideal OPV device is assumed to have negligible reflectance, meaning its CF-weighted LUE is an upper estimate. We also note that the addition of an AR coating to the optically modeled device would reduce the reflectance and improve transmission, though its performance without such a coating is already commendable. The use of a single-layer AR coating can reduce reflectance at the air-substrate interface by up to 5%.^[101,102] The performance of the AR coating can be improved by instead using a double-layer or multilayer gradient film approach, with the caveat of increased fabrication complexity and costs.^[103]

From the perspective of optimizing agrivoltaics at the systems level, the refractive index (n_{AR}) and thickness (d_{AR}) of a single-layer AR coating could be selected to minimize reflection at a desired wavelength (λ) using $n_{AR}(\lambda) = \sqrt{n_{air}(\lambda)n_{sub}(\lambda)}$ and $d_{AR} = \lambda/4n_{AR}(\lambda)$, respectively, where $n_{air}(\lambda)$ and $n_{sub}(\lambda)$ are the wavelength-dependent refractive index of air and the substrate, respectively.^[103] Thus, if a crop is known to depend vitally

on a particular wavelength, the AR coating can be tailored to prioritize transmission of this wavelength.

2.6. Case Study: Horticultural Greenhouses in the Netherlands

With the LUEs of agrivoltaics devices based on several material prescriptions established under AM1.5 G illumination, a final investigation was conducted utilizing real-world solar irradiance and temperature data. For this case study, the town of Naaldwijk (latitude = 51.99°N, longitude = 4.21°E) in the Westland municipality of the Netherlands, renowned for its horticultural greenhouses, was selected. To evaluate PV performance at this location, we expanded an open-source computational tool (PV-Sim) we developed for a prior work^[59,60] to incorporate a freely available database of around 45000 population centers.^[104] Furthermore, the ability to use application programming interface (API) calls to request irradiance and temperature data from the National Solar Radiation Database (NSRDB), hosted by the National Renewable Energy Laboratory (NREL), was added.^[105–107] Using API calls in this way reduces hardware requirements for End Users, as large quantities of data do not need to be stored in PV-Sim. An internet connection, however, is required. We note that similar tools are available, including the Photovoltaic Geographical Information System, which has been providing public access to data and PV performance predictions for over twenty years.^[108,109] PV-Sim, however, enables estimation of annual power generation while accounting for device-level parameters, including series and shunt resistances, ΔV_{oc}^{nr} losses, and perhaps most importantly, customizable material choices (End Users may select a measured EQE_{PV} spectrum from a database of dozens, or input their own). As far as we are aware, the ability to customize the PV material in such computational tools (beyond a handful of conventional materials like c-Si) was previously lacking. Thus, PV-Sim enables comparisons between next-generation PVs (such as OPVs and perovskites) and conventional PV materials.

To demonstrate the utility of geo-meteorological modeling using PV-Sim, we predicted PV performance for the six device models considered in Figure 7, with the results summarized in Figure 8. Therein, the global horizontal irradiance (GHI), which

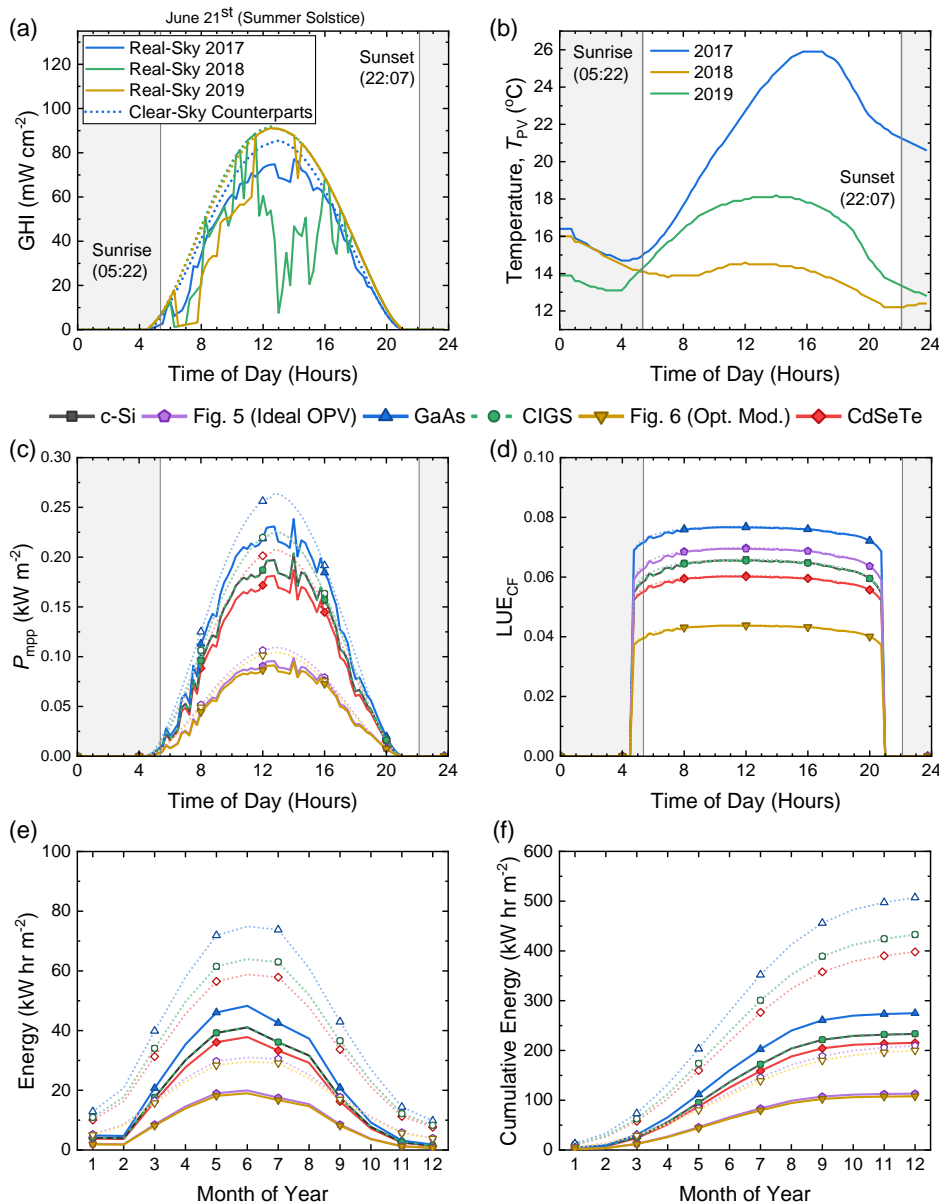


Figure 8. Simulating annual PV performance using solar insolation and temperature obtained from NREL's NSRDB for the town of Naaldwijk (51.99°N, 4.21°E) in the Netherlands. In (a) and (b), respectively, the GHI and ambient temperature are plotted as a function of time of day at the summer solstice (June 21st), for the years 2017, 2018, and 2019. For six different models of PV performance (c-Si – black squares; optimal $d = 100$ nm Ideal OPV from Figure 5 – purple pentagons; GaAs – blue triangles; CIGS – green circles; optimal $d = 100$ nm optically modeled OPV from Figure 6 – inverted, golden triangles; CdSeTe – red diamonds) the maximum power generated per square meter (P_{mpp}) and LUE_{CF} are plotted for the summer solstice in the year 2017, in (c) and (d), respectively. Furthermore, in each of these six cases, the total energy generated per month (in units of kW hour m⁻²), and the cumulative energy generated throughout the year are plotted in (e) and (f), respectively. In (c)–(f), the dotted lines with empty symbols correspond to the hypothetical “clear-sky” case, where PV performance is not impeded by cloud cover.

is the sum of the normal irradiance and the diffuse irradiance impinging on a surface parallel with the Earth's surface (corresponding to a horizontal roof), is plotted in Figure 8a against the time of day during the summer solstice (June 21st), for the years 2017, 2018, and 2019; the corresponding ambient temperature (T_{PV}) is plotted in Figure 8b. In Figure 8a, both the real-sky and clear-sky GHIs are plotted, with the former accounting for the shading and light-diffusing effects of clouds. For the

six device models considered in Section 2.5, the maximum power generated per unit area (P_{mpp}) in the thermodynamic limit (neglecting resistive losses) is plotted in Figure 8c for the summer solstice in 2017, with the corresponding LUE_{CF} plotted in Figure 8d. From these panels, one can see that while some inorganic materials generate more power per unit (e.g., CIGS), the CF-weighted LUE is enhanced for the optimal-thickness ideal OPV device considered in Figure 5; further emphasizing the

trade-off between light transmission and power generation. We note that, in the thermodynamic limit, c-Si and CIGS have very similar outputs, and so the latter is plotted with a dashed line to distinguish between them. Following this, the annual energy generation was determined for the year 2017 and plotted in Figure 8e, with the cumulative energy generation plotted in Figure 8f. From Figure 8, it is evident that the material choice will greatly affect the energy generated per square meter per annum, with the GaAs device generating 275 kW hr m^{-2} (under “real-sky” conditions), compared with the optimal-thickness, optically modeled OPV device generating just 100 kW hr m^{-2} . It is also clear that the shading and light-diffusing effects of clouds greatly reduce annual PV output; the GaAs device could generate over 500 kW hr m^{-2} under the hypothetical “clear-sky” conditions.

Using PV-Sim, investigations like the one presented in Figure 8 can be conducted for a variety of material choices, device parameters, locations, and more. Thus, PV-Sim could be used to inform further techno-economic analyses by incorporating a thermodynamic understanding of device performance under realistic conditions. Further enhancements that could be made to PV-Sim to inform systems-level analyses include allowing for tilted roofs and wall-mounted semitransparent PVs (alongside the associated angular dependence of the optics),^[110,111] heating and cooling (including cooling by wind, which could make use of windspeed data also supplied by the NSRDB),^[112,113] and accounting for the additional power generation arising from the back-scattering of light into the semitransparent PVs by the contents of the protected cropping environment (using the spectral albedo of the crop, soil, etc.),^[96,97,114,115] which, as previously mentioned, could increase the energy output by up to 20–25%.^[91,92]

3. Conclusion

In summary, while the maximum PCE for an OPV device has recently reached 20% under AM1.5 G illumination, the trade-off between light transmission and absorption for agrivoltaic applications requires that EQE_{PV} be minimized in the visible region of the electromagnetic spectrum, such that the LUE may be maximized. Using optical transfer matrix modeling and thermodynamic limit calculations, it was found that this trade-off requires the active layers of semitransparent OPVs to be around 100 nm thick for optimal agrivoltaic performance. However, the exact thickness required will depend on the optical and transport properties of a given device architecture, though charge can usually be efficiently collected for d up to 300 nm in OPVs.^[116]

Following this, we defined a CF with which PV cells occupy the roof of a protected cropping environment (such as a greenhouse). This factor was used to compare the CF-weighted LUEs of semitransparent OPVs with those of opaque, inorganic PVs that are spaced apart. We found that provided a semitransparent PV device’s above-gap EQE_{PV} is maximal for $E \leq 1.77 \text{ eV}$ and minimal elsewhere, the performance of OPVs (including reflectance and nonradiative voltage losses) is on par with inorganic PV cells at the optimal CF of 50%. Of course, several other considerations could inform material choices for agrivoltaic devices,

including the stability of the device, the robustness of the protected cropping environment (i.e., whether it can support the weight of c-Si PVs), the local climate, the time of the year, the wavelength-sensitivity of the crop, and so on. It is never just a matter of maximizing transmission and power generation.

Further systems-level work, which the PV-Sim tool we presented in this work can support, could aim to account for additional degrees-of-freedom associated with agrivoltaic devices, with the ultimate goal of a full techno-economic description. Not only could this include lifecycle analysis of the chosen PV technology, where factors such as cost, ease-of-manufacture (and its associated carbon footprint), and durability will play a role, but it could also include considerations of the performance of PV modules and arrays, with the spacing between—and tilt angle of—each module being critical metrics for PV performance and crop growth. Many optical degrees-of-freedom could also be optimized, such as the thickness and material choices of AR coatings, and specific OPV systems being matched to particular crops based on their wavelength-selectivity requirements. To this end, the PV-Sim tool could allow for this wavelength selectivity to be integrated, as a starting point, into any systems-level approach to agrivoltaics. To demonstrate the utility of the open-source PV-Sim tool, we analyzed real-world irradiance and temperature data to predict the annual energy generation per square meter of PV material for a variety of material choices, while accounting for intrinsic features, including band-filling effects, radiative open-circuit voltage losses induced by subgap absorption, and nonradiative open-circuit voltage losses. Overall, we found that state-of-the-art, inorganic PVs generate more power per square meter than semitransparent OPVs, but the CF-weighted LUEs of OPVs can compete with established inorganic systems.

Supporting Information

Supporting Information is available from the Wiley Online Library or from the author.

Acknowledgements

This work was funded through the Welsh Government’s Sêr Cymru II Program “Sustainable Advanced Materials” (Welsh European Funding Office – European Regional Development Fund). P.M. is a Sêr Cymru II Research Chair and A.A. was a Rising Star Fellow also funded through the Welsh Government’s Sêr Cymru II “Sustainable Advanced Materials” Program (European Regional Development Fund, Welsh European Funding Office, and Swansea University Strategic Initiative). This work was also funded by UKRI through the EPSRC Program Grant EP/T028513/1 Application Targeted and Integrated Photovoltaics and the UKRI Research England RPIF Programme (Centre for Integrative Semiconductor Materials). O.J.S. is an Academy Research Fellow and acknowledges funding from the Research Council of Finland through project #357196. The authors would also like to acknowledge fruitful discussions with Professor Ben Hankamer (University of Queensland, Centre for Solar Biotechnology), Professor Harald Ade (North Carolina State University, Department of Physics), and Dr. Kieran Richards (Swansea University, Department of Chemistry).

Conflict of Interest

The authors declare no conflict of interest.

Data Availability Statement

The data that support the findings of this study are available from the corresponding author upon reasonable request.

Keywords

agrivoltaics, average visible transmission, organic semiconductors, photovoltaics, power conversion efficiency, semitransparent photovoltaics

Received: June 22, 2024

Revised: July 17, 2024

Published online: August 26, 2024

- [1] O. Almora, D. Baran, G. C. Bazan, C. Berger, C. I. Cabrera, K. R. Catchpole, S. Erten-Ela, F. Guo, J. Hauch, A. W. Y. Ho-Baillie, T. J. Jacobsson, R. A. J. Janssen, T. Kirchartz, N. Kopidakis, Y. Li, M. A. Loi, R. R. Lunt, X. Mathew, M. D. McGehee, J. Min, D. B. Mitzi, M. K. Nazeeruddin, J. Nelson, A. F. Nogueira, U. W. Paetzold, N.-G. Park, B. P. Rand, U. Rau, H. J. Snaith, E. Unger, et al., *Adv. Energy Mater.* **2021**, *11*, 2102526.
- [2] O. Almora, D. Baran, G. C. Bazan, C. I. Cabrera, S. Erten-Ela, K. Forberich, F. Guo, J. Hauch, A. W. Y. Ho-Baillie, T. J. Jacobsson, R. A. J. Janssen, T. Kirchartz, N. Kopidakis, M. A. Loi, R. R. Lunt, X. Mathew, M. D. McGehee, J. Min, D. B. Mitzi, M. K. Nazeeruddin, J. Nelson, A. F. Nogueira, U. W. Paetzold, B. P. Rand, U. Rau, H. J. Snaith, E. Unger, L. Vaillant-Roca, C. Yang, H.-L. Yip, et al., *Adv. Energy Mater.* **2023**, *13*, 2203313.
- [3] M. A. Green, E. D. Dunlop, M. Yoshita, N. Kopidakis, K. Bothe, G. Siefer, X. Hao, *Prog. Photovolt.: Res. Appl.* **2024**, *32*, 3.
- [4] R. Arshad, S. Zahoor, M. A. Shah, A. Wahid, H. Yu, *IEEE Access* **2017**, *5*, 15667.
- [5] Y. Cui, L. Hong, J. Hou, *ACS Appl. Mater. Interfaces* **2020**, *12*, 38815.
- [6] G. Burwell, O. J. Sandberg, W. Li, P. Meredith, M. Carnie, A. Armin, *Sol. RRL* **2022**, *6*, 2200315.
- [7] B. Lee, L. Lahann, Y. Li, S. R. Forrest, *Sustainable Energy Fuels* **2020**, *4*, 5765.
- [8] L. K. Reb, M. Böhmer, B. Predeschly, S. Grott, C. L. Weindl, G. I. Ivandekic, R. Guo, C. Dreißigacker, R. Gernhäuser, A. Meyer, *Joule* **2020**, *4*, 1880.
- [9] I. Cardinaletti, T. Vangerven, S. Nagels, R. Cornelissen, D. Schreurs, J. Hruby, J. Vodnik, D. Devisscher, J. Kesters, J. D'Haen, *Sol. Energy Mater. Sol. Cells* **2018**, *182*, 121.
- [10] H. Dinesh, J. M. Pearce, *Renewable Sustainable Energy Rev.* **2016**, *54*, 299.
- [11] C. Dupraz, H. Marrou, G. Talbot, L. Dufour, A. Nogier, Y. Ferard, *Renewable Energy* **2011**, *36*, 2725.
- [12] M. A. Al Mamun, P. Dargusch, D. Wadley, N. A. Zulkarnain, A. A. Aziz, *Renewable Sustainable Energy Rev.* **2022**, *161*, 112351.
- [13] D. Tilman, C. Balzer, J. Hill, B. L. Befort, *Proc. Natl. Acad. Sci.* **2011**, *108*, 20260.
- [14] *European Commission: Agrivoltaics Alone Could Surpass EU Photovoltaic 2030 Goals* **2023**, https://joint-research-centre.ec.europa.eu/jrc-news-and-updates/agrivoltaics-alone-could-surpass-eu-photovoltaic-2030-goals-2023-10-12_en (accessed: 02 February 2024).
- [15] P. Xue, P. Cheng, R. P. Han, X. Zhan, *Mater. Horiz.* **2022**, *9*, 194.
- [16] R. Abbel, Y. Galagan, P. Groen, *Adv. Eng. Mater.* **2018**, *20*, 1701190.
- [17] R. Patidar, D. Burkitt, K. Hooper, D. Richards, T. Watson, *Mater. Today Commun.* **2020**, *22*, 100808.
- [18] M. K. H. Rabaia, C. Semeraro, A.-G. Olabi, *J. Clean. Prod.* **2022**, *373*, 133864.
- [19] G. A. Heath, T. J. Silverman, M. Kempe, M. Deceglie, D. Ravikumar, T. Remo, H. Cui, P. Sinha, C. Libby, S. Shaw, *Nat. Energy* **2020**, *5*, 502.
- [20] M. Charles, B. Edwards, E. Ravishankar, J. Calero, R. Henry, J. Rech, C. Saravitz, W. You, H. Ade, B. O'Connor, *Beyond Energy Balance in Agrivoltaic Food Production: Emergent Crop Traits from Color Selective Solar Cells*, *bioRxiv*, **2022**: p. 2022.03. 10.482833.
- [21] R. Meitzner, U. S. Schubert, H. Hoppe, *Adv. Energy Mater.* **2021**, *11*, 2002551.
- [22] W. Song, J. Ge, L. Xie, Z. Chen, Q. Ye, D. Sun, J. Shi, X. Tong, X. Zhang, Z. Ge, *Nano Energy* **2023**, *116*, 108805.
- [23] C. J. Emmott, J. A. Röhr, M. Campoy-Quiles, T. Kirchartz, A. Urbina, N. J. Ekins-Daukes, J. Nelson, *Energy Environ. Sci.* **2015**, *8*, 1317.
- [24] I. Moons, P. De Pelsmacker, A. Pijnenburg, K. Daems, L. J. Van de Velde, *J. Clean. Prod.* **2022**, *330*, 129752.
- [25] R. L. Cook, *Greenhouse Tomatoes Change The Dynamics of the North American Fresh Tomato Industry*, Vol. 2, US Department of Agriculture, Economic Research Service **2005**.
- [26] J. J. Hanan, *Greenhouses: Advanced Technology For Protected Horticulture*, CRC Press, Boca Raton, FL **2017**.
- [27] E. Sisbon, *Hungry Sheep Help Save Money at University of Queensland Solar Research Farm* **2016**, <https://www.abc.net.au/news/2016-08-15/uq-uses-sheep-to-cut-grass-at-gatton-solar-research-farm/7734770>.
- [28] M. Charles, B. Edwards, E. Ravishankar, J. Calero, R. Henry, J. Rech, C. Saravitz, W. You, H. Ade, B. O'Connor, *Front. Plant Sci.* **2023**, *14*, 1087707.
- [29] S. Eichhorn Bilodeau, B.-S. Wu, A.-S. Rufyikiri, S. MacPherson, M. Lefsrud, *Front. Plant Sci.* **2019**, *10*, 296.
- [30] R. Wimalasekera, *Photosynthesis, Productivity and Environmental Stress*, Wiley, Hoboken, NJ **2019**, pp. 65–73.
- [31] E. Sakshaug, A. Bricaud, Y. Dandonneau, P. G. Falkowski, D. A. Kiefer, L. Legendre, A. Morel, J. Parslow, M. Takahashi, *J. Plankton Res.* **1997**, *19*, 1637.
- [32] S. G. Chavan, C. Maier, Y. Alagoz, J. C. Filipe, C. R. Warren, H. Lin, B. Jia, M. E. Loik, C. I. Cazzonelli, Z. H. Chen, *Food Energy Sec.* **2020**, *9*, e245.
- [33] P. G. Kevan, L. Chittka, A. G. Dyer, *J. Exp. Biol.* **2001**, *204*, 2571.
- [34] D. Stavenga, R. Smits, B. Hoenders, *Vis. Res.* **1993**, *33*, 1011.
- [35] T. Sekiyama, A. Nagashima, *Environments* **2019**, *6*, 65.
- [36] Y. Cui, C. Yang, H. Yao, J. Zhu, Y. Wang, G. Jia, F. Gao, J. Hou, *Adv. Mater.* **2017**, *29*, 1703080.
- [37] M. R. Filip, G. E. Eperon, H. J. Snaith, F. Giustino, *Nat. Commun.* **2014**, *5*, 5757.
- [38] T. M. Clarke, J. R. Durrant, *Chem. Rev.* **2010**, *110*, 6736.
- [39] A. Köhler, H. Bässler, *Electronic Processes in Organic Semiconductors: An Introduction*, John Wiley & Sons, Hoboken, NJ **2015**.
- [40] C. Deibel, T. Strobel, V. Dyakonov, *Adv. Mater.* **2010**, *22*, 4097.
- [41] L. Zhu, M. Zhang, G. Zhou, T. Hao, J. Xu, J. Wang, C. Qiu, N. Prine, J. Ali, W. Feng, *Adv. Energy Mater.* **2020**, *10*, 1904234.
- [42] F. D. Eisner, M. Azzouzi, Z. Fei, X. Hou, T. D. Anthopoulos, T. J. S. Dennis, M. Heeney, J. Nelson, *J. Am. Chem. Soc.* **2019**, *141*, 6362.
- [43] J. Yan, E. Rezasoltani, M. Azzouzi, F. Eisner, J. Nelson, *Nat. Commun.* **2021**, *12*, 3642.
- [44] M. A. Green, E. D. Dunlop, G. Siefer, M. Yoshita, N. Kopidakis, K. Bothe, X. Hao, *Prog. Photovolt.: Res. Appl.* **2003**, *31*, 3.
- [45] L. Zhu, M. Zhang, J. Xu, C. Li, J. Yan, G. Zhou, W. Zhong, T. Hao, J. Song, X. Xue, Z. Zhou, R. Zeng, H. Zhu, C.-C. Chen, R. C. I. MacKenzie, Y. Zou, J. Nelson, Y. Zhang, Y. Sun, F. Liu, *Nat. Mater.* **2022**, *21*, 656.
- [46] O. J. Sandberg, A. Armin, *J. Phys. Chem. C* **2021**, *125*, 15590.
- [47] Y. Sun, L. Wang, C. Guo, J. Xiao, C. Liu, C. Chen, W. Xia, Z. Gan, J. Cheng, J. Zhou, Z. Chen, J. Zhou, D. Liu, T. Wang, W. Li, *J. Am. Chem. Soc.* **2024**, *146*, 12011.

- [48] A. Armin, W. Li, O. J. Sandberg, Z. Xiao, L. Ding, J. Nelson, D. Neher, K. Vandewal, S. Shoaee, T. Wang, H. Ade, T. Heumüller, C. Brabec, P. Meredith, *Adv. Energy Mater.* **2021**, *11*, 2003570.
- [49] J. Hou, O. Inganäs, R. H. Friend, F. Gao, *Nat. Mater.* **2018**, *17*, 119.
- [50] M. B. Faheem, B. Khan, C. Feng, S. B. Ahmed, J. Jiang, M.-U. Rehman, W. Subhani, M. Farooq, J. Nie, M. Makhoulouf, *ACS Appl. Mater. Interfaces* **2022**, *14*, 6894.
- [51] M. A. Green, A. Ho-Baillie, H. J. Snaith, *Nat. Photonics* **2014**, *8*, 506.
- [52] B. Shi, L. Duan, Y. Zhao, J. Luo, X. Zhang, *Adv. Mater.* **2020**, *32*, 1806474.
- [53] J. Seo, J. H. Noh, S. I. Seok, *Acc. Chem. Res.* **2016**, *49*, 562.
- [54] L. A. Pettersson, L. S. Roman, O. Inganäs, *J. Appl. Phys.* **1999**, *86*, 487.
- [55] P. Peumans, A. Yakimov, S. R. Forrest, *J. Appl. Phys.* **2003**, *93*, 3693.
- [56] E. Centurioni, *Appl. Opt.* **2005**, *44*, 7532.
- [57] G. F. Burkhard, E. T. Hoke, M. D. McGehee, *Adv. Mater.* **2010**, *22*, 3293.
- [58] G. F. Burkhard, E. T. Hoke, *Transfer Matrix Optical Modeling*, McGehee Group (Stanford University) **2011**.
- [59] A. M. Kay, *Photovoltaic Performance Simulator 2024*, https://github.com/Austin-M-Kay/Photovoltaic_Performance_Simulator.
- [60] A. M. Kay, M. E. Fitzsimons, G. Burwell, P. Meredith, A. Armin, O. J. Sandberg, *Sol. RRL* **2023**, *7*, 2300277.
- [61] W. Shockley, H. J. Queisser, *J. Appl. Phys.* **1961**, *32*, 510.
- [62] M. Azzouzi, J. Yan, T. Kirchartz, K. Liu, J. Wang, H. Wu, J. Nelson, *Phys. Rev. X* **2018**, *8*, 031055.
- [63] J. Benduhn, K. Tvingstedt, F. Piersimoni, S. Ullbrich, Y. Fan, M. Tropiano, K. A. McGarry, O. Zeika, M. K. Riede, C. J. Douglas, S. Barlow, S. R. Marder, D. Neher, D. Spoltore, K. Vandewal, *Nat. Energy* **2017**, *2*, 17053.
- [64] F. Urbach, *Phys. Rev.* **1953**, *92*, 1324.
- [65] A. M. Kay, O. J. Sandberg, N. Zarrabi, W. Li, S. Zeiske, C. Kaiser, P. Meredith, A. Armin, *Adv. Funct. Mater.* **2022**, *32*, 2113181.
- [66] C. Kaiser, O. J. Sandberg, N. Zarrabi, W. Li, P. Meredith, A. Armin, *Nat. Commun.* **2021**, *12*, 3988.
- [67] J. Wong, S. T. Omelchenko, H. A. Atwater, *ACS Energy Lett.* **2020**, *6*, 52.
- [68] P. Würfel, *J. Phys. C: Solid State Phys.* **1982**, *15*, 3967.
- [69] P. Würfel, U. Würfel, *Physics of Solar Cells: From Basic Principles to Advanced Concepts*, John Wiley & Sons, Hoboken, NJ **2016**.
- [70] S. Ullbrich, J. Benduhn, X. Jia, V. C. Nikolis, K. Tvingstedt, F. Piersimoni, S. Roland, Y. Liu, J. Wu, A. Fischer, D. Neher, S. Reineke, D. Spoltore, K. Vandewal, *Nat. Mater.* **2019**, *18*, 459.
- [71] X.-K. Chen, D. Qian, Y. Wang, T. Kirchartz, W. Tress, H. Yao, J. Yuan, M. Hülsbeck, M. Zhang, Y. Zou, Y. Sun, Y. Li, J. Hou, O. Inganäs, V. Coropceanu, J.-L. Bredas, F. Gao, *Nat. Energy* **2021**, *6*, 799.
- [72] J.-W. Lee, C. Sun, T. N.-L. Phan, D. C. Lee, Z. Tan, H. Jeon, S. Cho, S.-K. Kwon, Y.-H. Kim, B. J. Kim, *Energy Environ. Sci.* **2023**, *16*, 3339.
- [73] J. Fu, P. W. K. Fong, H. Liu, C.-S. Huang, X. Lu, S. Lu, M. Abdelsamie, T. Kodalle, C. M. Sutter-Fella, Y. Yang, G. Li, *Nat. Commun.* **2023**, *14*, 1760.
- [74] S. M. Hosseini, S. Wilken, B. Sun, F. Huang, S. Y. Jeong, H. Y. Woo, V. Coropceanu, S. Shoaee, *Adv. Energy Mater.* **2023**, *13*, 2203576.
- [75] Y. Zhang, S. Yuan, C. Zhang, C. Ding, C. Zhang, H. Xu, *Materials* **2023**, *16*, 5620.
- [76] Q. Shen, C. He, B. Wu, Y. Lin, S. Chen, J. Gao, S. Li, Z. Ma, W. Ma, M. Shi, Y. Li, H. Chen, *Chem. Eng. J.* **2023**, *471*, 144472.
- [77] R. Suthar, A. T. H. Dahiya, A. K. Singh, G. D. Sharma, S. Karak, *ACS Appl. Mater. Interfaces* **2023**, *15*, 3214.
- [78] K. Yang, Y. Chang, Y. Chang, K. Lyu, Z. Wei, *J. Funct. Polym.* **2023**, *36*, 321.
- [79] Z. Jia, Q. Ma, Z. Chen, L. Meng, N. Jain, I. Angunawela, S. Qin, X. Kong, X. Li, Y. Yang, H. Zhu, H. Ade, F. Gao, Y. Li, *Nat. Commun.* **2023**, *14*, 1236.
- [80] P. Kaienburg, H. Bristow, A. Jungbluth, I. Habib, I. McCulloch, D. Beljonne, M. Riede, *ACS Appl. Mater. Interfaces* **2023**, *15*, 31684.
- [81] B. Liu, S. Liang, S. Karuthedath, Y. He, J. Wang, W. L. Tan, H. Li, Y. Xu, F. Laqui, C. J. Brabec, C. R. McNeill, C. Xiao, Z. Tang, J. Hou, F. Yang, W. Li, *Macromolecules* **2023**, *56*, 1154.
- [82] U. Rau, *Phys. Rev. B* **2007**, *76*, 085303.
- [83] N. Zarrabi, O. J. Sandberg, S. Zeiske, W. Li, D. B. Riley, P. Meredith, A. Armin, *Nat. Commun.* **2020**, *11*, 5567.
- [84] T. Xu, B. Deng, Y. Zhao, Z. Wang, G. Lévêque, Y. Lambert, B. Grandidier, S. Wang, F. Zhu, *Adv. Energy Mater.* **2023**, *13*, 2301367.
- [85] B. E. Trembl, T. Hanrath, *ACS Energy Lett.* **2016**, *1*, 391.
- [86] P. R. Boyce, *Human Factors in Lighting*, 3rd ed, CRC Press, Boca Raton **2014**.
- [87] C. Yang, D. Liu, M. Bates, M. C. Barr, R. R. Lunt, *Joule* **2019**, *3*, 1803.
- [88] C. J. Traverse, R. Pandey, M. C. Barr, R. R. Lunt, *Nat. Energy* **2017**, *2*, 849.
- [89] Y. Zhao, Y. Zhu, H.-W. Cheng, R. Zheng, D. Meng, Y. Yang, *Mater. Today Energy* **2021**, *22*, 100852.
- [90] R. Kerremans, C. Kaiser, W. Li, N. Zarrabi, P. Meredith, A. Armin, *Adv. Opt. Mater.* **2020**, *8*, 2000319.
- [91] K. Jäger, P. Tillmann, C. Becker, *Opt. Express* **2020**, *28*, 4751.
- [92] U. A. Yusufoglu, T. M. Pletzer, L. J. Koduvellikulathu, C. Comparotto, R. Kopecek, H. Kurz, *IEEE J. Photovolt.* **2014**, *5*, 320.
- [93] M. H. Riaz, H. Imran, H. Alam, M. A. Alam, N. Z. Butt, *IEEE J. Photovolt.* **2022**, *12*, 572.
- [94] M. H. Riaz, H. Imran, R. Younas, M. A. Alam, N. Z. Butt, *IEEE J. Photovolt.* **2021**, *11*, 469.
- [95] D. J. Griffiths, *Am. J. Phys.* **2005**, *73*, 574.
- [96] S. Idso, R. Jackson, R. Reginato, B. Kimball, F. Nakayama, *J. Appl. Meteorol. Climatol.* **1975**, *14*, 109.
- [97] A. Matthias, A. Fimbres, E. Sano, D. Post, L. Accioly, A. Batchily, L. Ferreira, *Soil Sci. Soc. Am. J.* **2000**, *64*, 1035.
- [98] J. C. Blakesley, G. Koutsourakis, D. E. Parsons, N. A. Mica, S. Balasubramanyam, M. G. Russell, *Sol. Energy* **2023**, *266*, 112144.
- [99] R. Kopecek, J. Libal, *Energies* **2021**, *14*, 2076.
- [100] R. Mallick, X. Li, C. Reich, X. Shan, W. Zhang, T. Nagle, L. Bok, E. Bicakci, N. Rosenblatt, D. Modi, R. Farshchi, C. Lee, J. Hack, S. Grover, N. Wolf, W. K. Metzger, D. Lu, G. Xiong, *IEEE J. Photovolt.* **2023**, *13*, 510.
- [101] Y. Wang, M. Chen, D. Li, Z. Huang, Y. Mao, W. Han, T. Wang, D. Liu, *J. Mater. Chem. C* **2019**, *7*, 14962.
- [102] K. Forberich, G. Dennler, M. C. Scharber, K. Hingerl, T. Fromherz, C. J. Brabec, *Thin Solid Films* **2008**, *516*, 7167.
- [103] M. Keshavarz Hedayati, M. Elbahri, *Materials* **2016**, *9*, 497.
- [104] *World Cities Database 2024*, <https://simplemaps.com/data/world-cities> (accessed: 09 January 2024).
- [105] M. Sengupta, Y. Xie, A. Lopez, A. Habte, G. Maclaurin, J. Shelby, *Renewable Sustainable Energy Rev.* **2018**, *89*, 51.
- [106] A. Habte, M. Sengupta, A. Lopez, *Evaluation of the National Solar Radiation Database (NSRDB): 1998–2015*, National Renewable Energy Laboratory (NREL), Golden, CO (United States) **2017**.
- [107] NREL, National Renewable Energy Laboratory, NSRDB: National Solar Radiation Database **2024**, <https://nsrdb.nrel.gov/> (accessed: 20 January 2024).
- [108] M. Suri, T. Huld, T. Cebeauer, E. D. Dunlop, *IEEE J. Sel. Top. Appl. Earth Obs. Remote Sens.* **2008**, *1*, 34.
- [109] *Photovoltaic Geographical Information System 2024*, https://re.jrc.ec.europa.eu/pvg_tools/en/ (accessed: 25 February 2024).
- [110] M. Young, C. J. Traverse, R. Pandey, M. C. Barr, R. R. Lunt, *Appl. Phys. Lett.* **2013**, *103*, 133304.
- [111] P. E. Campana, B. Stridh, S. Amaducci, M. Colauzzi, *J. Clean. Prod.* **2021**, *325*, 129091.

- [112] L. Zhu, A. Raman, K. X. Wang, M. Abou Anoma, S. Fan, *Optica* **2014**, 1, 32.
- [113] N. Gökmen, W. Hu, P. Hou, Z. Chen, D. Sera, S. Spataru, *Renewable Energy* **2016**, 90, 283.
- [114] Q. Yang, X. Liu, W. Wu, *Sensors* **2020**, 20, 4456.
- [115] E. Graser, C. Van Bavel, *Agric. Meteorol.* **1982**, 27, 17.
- [116] W. Li, S. Zeiske, O. J. Sandberg, D. B. Riley, P. Meredith, A. Armin, *Energy Environ. Sci.* **2021**, 14, 6484.